 doi:10.20944/preprints202008.0477.v1

Article

Two-Objective Optimization of a Kaplan Turbine Draft Tube Using a Response Surface Methodology

Riccardo Orso[1], Ernesto Benini[1,*], Moreno Minozzo[2] and Riccardo Bergamin[2]

[1] University of Padua, Dept. of Industrial Engineering
[2] ZECO S.r.l.; {moreno.minozzo, riccardo.bergamin}@zeco.it
* Correspondence: ernesto.benini@unipd.it

Received: date; Accepted: date; Published: date

Abstract: The overall cost of a hydropower plant is mainly due to the expenses for civil works, mechanical equipment (turbine and control units) and electrical components. The goal of a new draft tube design is to obtain a geometry that reduces investment costs, especially the excavation ones, but the primary driver is to increase the overall machine efficiency allowing for reduced payback time. In the present study, an optimization study of the elbow-draft tube assembly of a Kaplan turbine was conducted. A CFD model for the complete turbine has been developed and validated; next, an optimization of the draft tube alone was performed using a Design of Experiments technique; finally, several optimum solutions for the draft tube were obtained using a Response Surface technique aiming at maximizing pressure recovery and minimizing flow losses. A selection of optimized geometries was subsequently post-checked using the validated model of the entire turbine and a detailed flow analysis on the obtained results could make it possible to provide insight into the improved designs. It was observed that efficiency could be improved by 1% (in relative terms), and the mechanical power increased by 1,8% (in relative terms) with respect to the baseline turbine.

Keywords: Kaplan turbine; draft tube optimization; CFD analysis; DOE; Response Surface

1. Introduction

In recent decades, environmental policies have been oriented towards reducing energetic dependence from fossil fuels, thus leading to renewed and increased investments in the hydroelectric sector; such investments have been primarily directed to optimizing both new designs and existing installations, thus allowing for more efficient plants and reduced pay-back times. Kaplan hydro turbines have been adopted for a long time to deal with efficient energy production in the range of high specific speeds [1]: in fact, staggering a movable vaned distributor and runner blades according to the net head and the flow rate that the machine is subject to makes Kaplan turbines able to limit incidence flow losses and ultimately leads to high conversion efficiency in a wide range of flow rates, from 40 to 120% of the nominal value. The main drawback of Kaplan turbines is that, as the flow rate gets higher, the size of the turbine increases and costs attributed to civil works become more and more substantial.

In these machines, the draft tube plays a fundamental role as it makes it possible to recover a significant fraction of the kinetic energy leaving the runner by conversion into static pressure. As it is well known, this ultimately leads to creating an additional suction head downstream of the runner and makes it possible to increase the effective head that the runner is able to deliver [2]. In addition, the draft tube plays a fundamental role in determining the turbine efficiency since the height at which the tube is installed contributes to a large percentage of the total net head which can be recovered. Moreover, it is one of the most challenging parts to analyze from a fluid flow perspective due to the

Preprints (www.preprints.org) | NOT PEER-REVIEWED | Posted: 21 August 2020 doi:10.20944/preprints202008.0477.v1

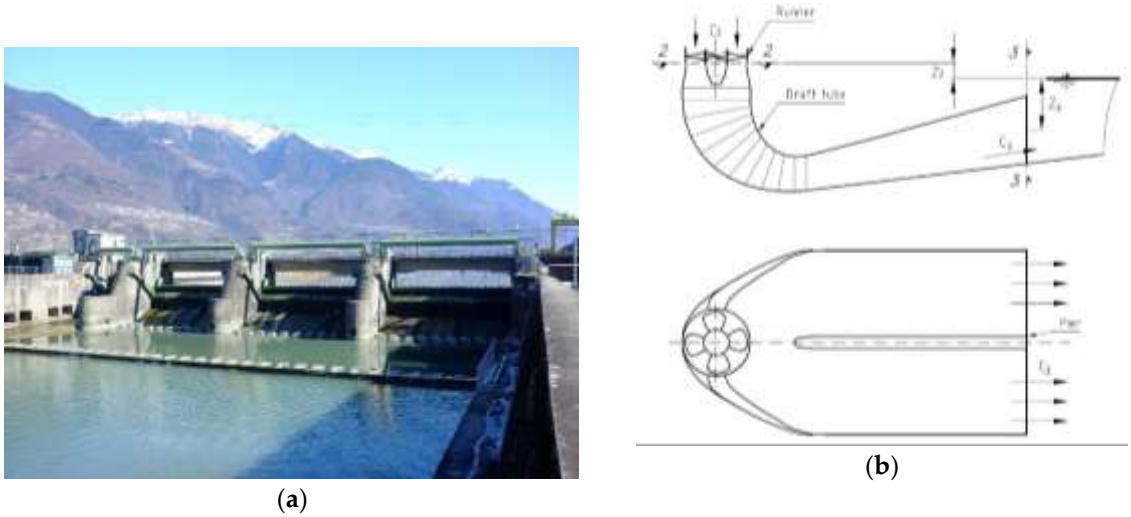

(**a**) (**b**)

Figure 1. Original power plant: (**a**) Overall external view; (**b**) Baseline elbow-drat tube geometry.

interaction of many complex flow features such as unsteadiness, turbulence, separation, curvature streamline, secondary flow, swirl, and vortex breakdown [3]. CFD studies of this component have been documented which make use of RANS-LES hybrid models (such as the scale-adaptive-simulation SST or the zonal-large-eddy-simulation) in [4-7]. These models can accurately predict turbulent phenomena in the draft tube but require very large computational resources. As such, the adoption of such models in optimization studies seems today still infeasible, while validated RANS approaches offer a very good compromise between accuracy and computational effort [2-3].

Past studies on draft tube optimizations were limited in terms of representativeness. In fact, while it has been demonstrated that the draft tube can be acceptably optimized as an isolated component around its design point [8-14], therefore neglecting the interference effects with the turbine runner, the performance of optimal configurations have not been post-checked using the entire turbine model for an *a posteriori* validation of the complete turbine installation.

In the present paper, a fully 3D Kaplan turbine RANS CFD model was first established and validated against available experimental data in terms of net head, flow rate, efficiency and mechanical power. Following this, the pressure and velocity distribution at the draft tube inlet were extracted from the previous computations. Finally, a CFD model that contained only the draft tube and its outlet extension was created and used in the optimization process. Unlike previous studies, the optimization study was carried out based on two-objectives which are of prominent interest to draft tube designers, i.e. its pressure recovery and its total pressure loss coefficient. Also, a noteworthy improvement with respect to past studies relies on the verification of the obtained results: in fact, once the optimal draft tube geometries have been found, they were tested back using the CFD model of full machine to find out their impact on the turbine efficiency and to analyze the sources of draft tube losses in detail.

2. Materials and Methods

2.1. Draft tube performance

The datum, or baseline, draft tube is connected to a Kaplan turbine runner installed in a 576-kW hydraulic power plant located in Adda river (Italy), as depicted in Figure 1(a). The original geometry adopted for the elbow draft tube is schematically represented in Figure 1(b). It is well known that, thanks to the draft tube, it is possible to recover part of the flow kinetic energy at sect. no. 2, i.e. downstream of the runner. To this purpose, the draft tube behaves as a diffuser featuring a prescribed area distribution along the equivalent centerline.

Two coefficients are used here to quantify the performance of a draft tube, namely a pressure recovery factor (Cp) and a drag coefficient (Cd), defined respectively as:

Preprints (www.preprints.org) | NOT PEER-REVIEWED | Posted: 21 August 2020 doi:10.20944/preprints202008.0477.v1

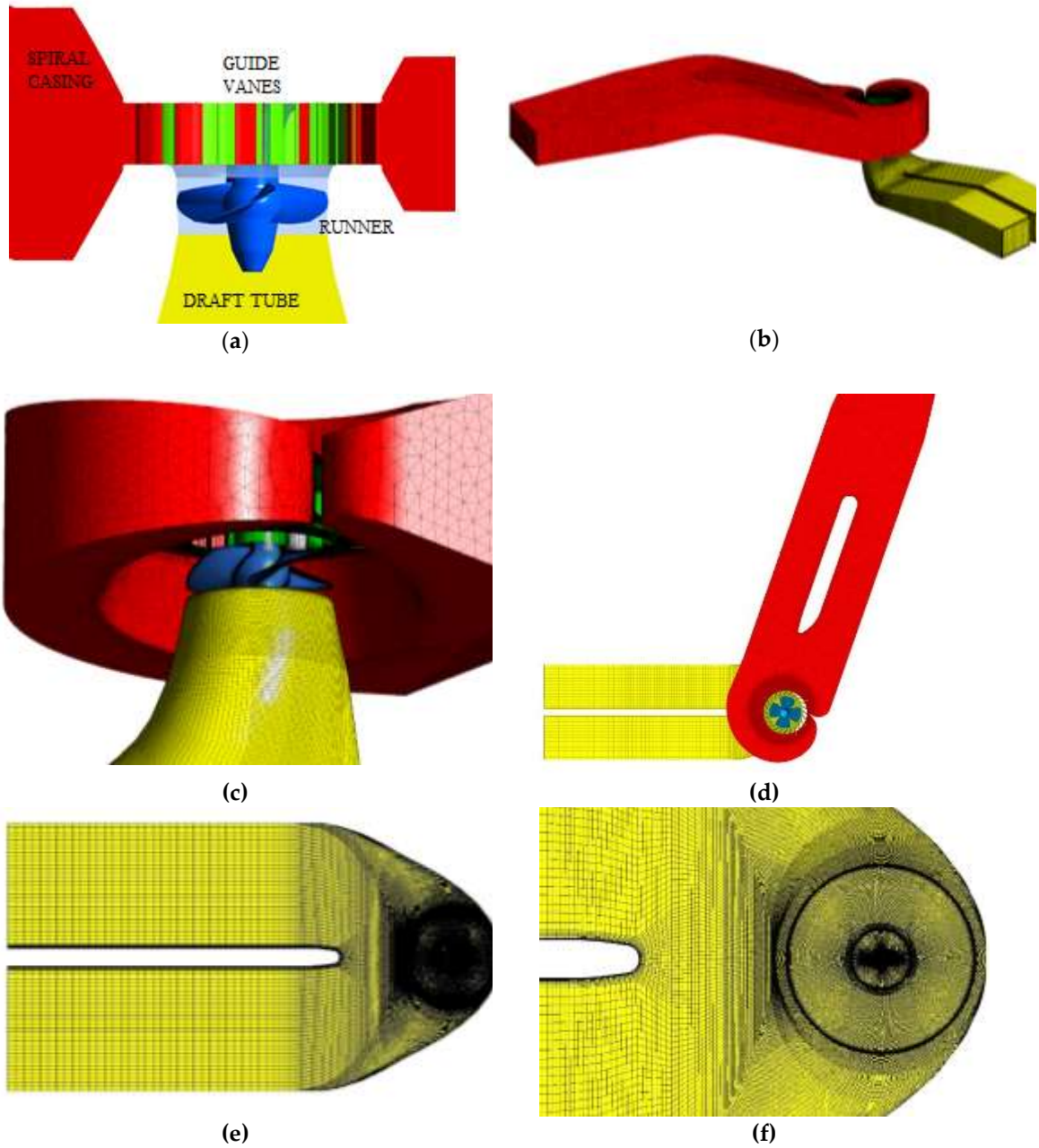

Figure 2. Turbine computational domains: (**a**) Close up of the runner domain in meridional view; (**b**) 3-D view of the overall domain; **(c)** Close up of the computational mesh in the region close to the runner/draft tube interface; **(d)** Top view of the overall domain, **(e), (f)** details of the draft tube mesh.

$$C_p = \frac{p_3 - p_2}{\frac{1}{2}\rho c_2^2}; \quad C_d = \frac{p_{tot-2} - p_{tot-3}}{\frac{1}{2}\rho c_2^2} \tag{1}$$

where p is the static pressure, p_{tot} the total pressure, subscripts 2 and 3 refer to the station downstream the runner and to the draft tube outlet respectively, ρ is the water density and c the absolute velocity.

Values of these coefficients are strictly related to the area distribution and are notoriously conflicting in such a way that the more intense is the diffusion (high Cp) the bigger is the head loss that might occur as a result of flow separation, secondary losses etc. (high Cd). Therefore, a good draft tube features the highest possible Cp along with the minimum achievable Cd. These two coefficients were used as objective functions in the multi-objective optimization study described later on.

 doi:10.20944/preprints202008.0477.v1

Table 1. Details of the grids used in the subdomains

Subdomain	Meshing tool	Mesh type	No. of nodes	No. of elements	Average y+
Spiral casing with stay vanes	ICEM-CFD	Tetra	2,580,807	7,685,535	62
Guide vanes	Turbogrid	Hexa	1,939,968	1,781,112	95
Distributor ring	ICEM-CFD	Hexa	478,720	462,672	28
Runner	Turbogrid	Hexa	1,023,320	964,180	110
Draft tube with extension	ICEM-CFD	Hexa	1,882,944	1,842,398	65

2.2. CFD model setup and validation

A steady-state RANS CFD model of the complete turbine was created which included the complete spiral casing with stay vanes, guide vanes, runner and draft tube (Figure 2). A mesh independency analysis led to the computational grids visible in Figure 2. Their details and statistics are provided in Table 1. As boundary conditions, a total pressure was defined at the inlet of the spiral casing and a static pressure equal to 0 Pa (relative to the atmospheric pressure value of 1 atm) was set at the outlet of the draft tube.

The total pressure at the inlet boundary corresponded to the total energy that the plant can process and was calculated from the net head and the flow rate that the turbine is subjected to. The Ansys CFX 19.2 solver was used to solve the RANS equations. Since the runner was not modelled as a rotating mesh, a Multiple-Reference-Frame approach was implemented and a mixing-plane condition was set both at the distributor-runner and runner-draft tube interfaces. Among all the turbulence models (all the variants of both k-ε and k-ω available in Ansys CFX 19.2 were actually tested), it was observed that the k-ω SST [15] provided the most accurate predictions but it was also the one that required the highest computational effort; for this reason, the k-ω SST was used in off-loop analyses on the complete machine model, while the standard k-ε was used in the optimization due to its cheaper usage. A physical timescale corresponding to 1° of runner rotation and a high-resolution scheme were set. In order to assure improved numerical stability, 50 iterations were ran at first using first-order schemes. These results were adopted as initial values for the high-resolution scheme run. During the convergence runs, several variables of interest were monitored, such as flow rate, efficiency, static pressure at draft tube inlet and mechanical power output. Final results were available after 3000 iterations on average and almost 72 hours of CPU calculations. All calculations were performed on a server equipped with Intel® Xeon® CPU x5650 processors using parallel solution on 10 multiple cores. Convergence was assessed when all variables of interest showed a variation lower than 0.08%.

Results from both experiments and simulations are in Figure 3. All the experimental data (net head, flow rate, efficiency and mechanical power) were taken in compliance with the European IEC EN 60041:1991 standard [16] and include the appropriate uncertainty bandwidth. Power and efficiency data from CFD are calculated respectively as follows:

Preprints (www.preprints.org) | NOT PEER-REVIEWED | Posted: 21 August 2020 doi:10.20944/preprints202008.0477.v1

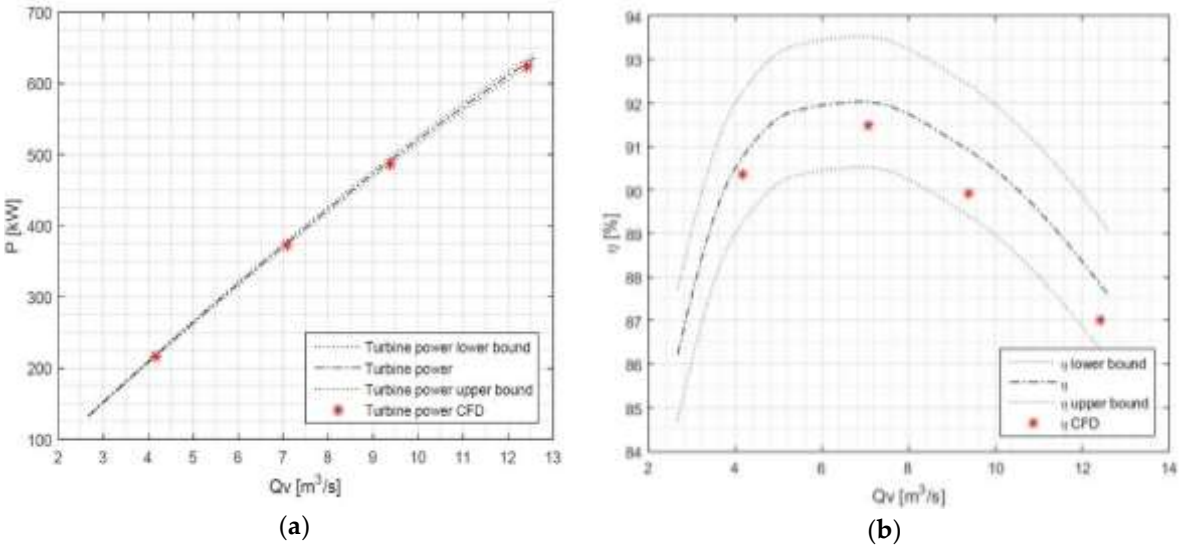

(**a**) (**b**)

Figure 3. Validation results: (**a**) Power data; (**b**) Efficiency.

$$P = M \cdot \omega;\ \eta = \frac{P}{\rho Q g H}$$

where M is the total torque on the runner blades, ω is the rotational speed, Q the flow rate and H the net head. As can be seen from Figure 3, power and efficiency data are within the experimental measurement uncertainty range. Thus, it can be concluded that the CFD model predicts the actual measured values with good accuracy and therefore, the model was considered validated. Furthermore, form the validation model it was possible to extract the runner-draft tube interface conditions. These are the velocity component distributions, i.e. the values of u, v, w (respectively tangential, absolute and relative velocity components) which could be used as inlet boundary conditions in the optimization process.

2.3. Draft tube geometry and parameterization

In Kaplan turbines, the draft tube geometry is quite complicated being the entrance cross-section circular due to the interface with the runner, while the exit cross-section is often of rectangular shape. Moreover, the draft tube features a 90° elbow to minimize excavation costs and to improve powerhouse compactness. As a result, a large number of design parameters are necessary to provide a successful geometry parameterization. In the present paper, the draft tube was parameterized using a mean line and a number of cross-sections stacked along the mean line.

The mean line was designed as composed by a first straight section, made by two segments, one related to the divergent cone, and one to the cylindrical section; then, a second curvilinear line is related to the elbow shape and is controlled by a three-point Bézier polygon. Finally, there is a segment connected to the last section of the draft tube. For the first straight part of the meanline, two parameters are involved, which are the two segments' length. For the Bézier polygon, four additional variables are introduced, which are the coordinates of the polygon-points (the coordinates of the first Bézier polygon point derive from the first straight part). Finally, one more parameter is added, that is the length of the last straight segment. Therefore, in the parameterization of the mean line, 7 variables are involved. The area distribution is managed using a 4th-degree polynomial as a function of the meanline coordinate x:

$$A(x) = P1 * (P2 * ax^4 + bx^3 + cx^2 + dx) + e \quad (2)$$

In Figure 4, the area distribution of the original geometry is represented using dots along with the polynomial interpolation. From the original geometry it was possible to obtain the polynomial coefficients (a, b, c, d, e) and use P1 and P2 as decision variables.

Preprints (www.preprints.org) | NOT PEER-REVIEWED | Posted: 21 August 2020 doi:10.20944/preprints202008.0477.v1

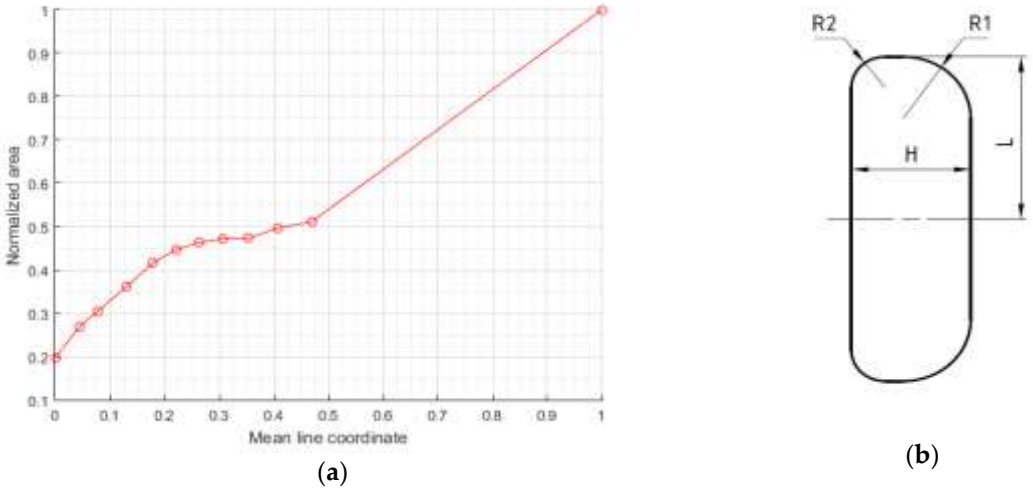

(**a**) (**b**)

Figure 4. Draft tube geometry definition: (**a**) Area distribution; (**b**) Shape of a generic cross section

Overall, the draft tube was parameterized using 9 decision variables. Regarding the shape of the draft tube sections, a clarification is needed. As already mentioned, the inlet section is circular, while the outlet is rectangular: in order not to increase the number of decision variables involved in the draft tube parameterization, it was decided to obtain the geometric relationship between the characteristic quantities from the original geometry and take advantage of the geometric similarity. In fact, for each section along the meanline, the geometric ratios R1/L, R2/L and H/L have been retained constant and equal to those of the baseline.

2.4. Optimization: problem formulation and tools

As previously mentioned, the optimization study was conducted on the draft tube alone by taking the inlet boundary conditions from the full machine model at the runner-draft tube interface. As a result, the flow domain included the runner discharge cone along with the runner-tube interface (which form the inlet boundary), the first divergent part, the elbow, the last divergent part and the draft tube prolongation leading to the outlet section.

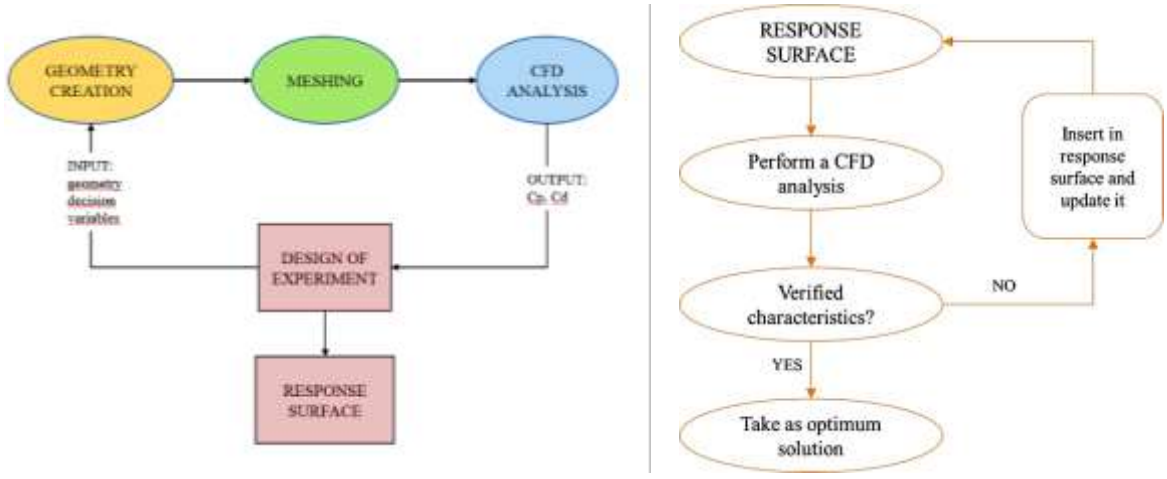

(**a**) (**b**)

Figure 5. Optimization procedure: (**a**) General loop; (**b**) Response surface update workflow.

Preprints (www.preprints.org) | NOT PEER-REVIEWED | Posted: 21 August 2020 doi:10.20944/preprints202008.0477.v1

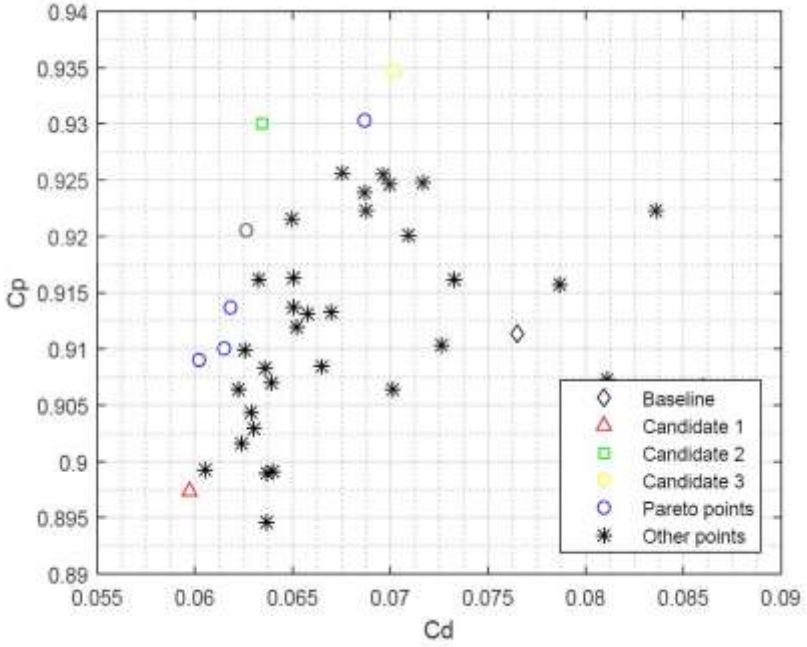

Figure 6. Optimization results: Pareto solutions

The optimization was a multi-objective one: the purpose was to maximize Cp and minimize Cd at the same time using a Pareto approach. As for the constraints, the optimization had to lead to solutions that were interchangeable with the baseline case currently installed without any modifications regarding the runner. As a result, during the entire procedure the baseline inlet and runner cone (both belonging to the runner) remained fixed. A further constraint was related to the global draft tube depth, that affects the costs of civil works. As for the outlet, the depth could vary in all directions but with the limit of always remaining with a certain margin under the free water surface of the tailrace.

A response surface methodology for optimization tool was used [17]. The first step was the design space exploration using design of experiments (DOE). With this tool it was possible to understand how design parameters are related to each other and which are the ones with the most significant influence on the two objectives. In this paper, a "Central Composite Design" (CCD) DOE technique was adopted which provided a screening set of 150 samples to determine the overall trends of the metamodel. The latter was finally achieved using the genetic aggregation method [18] and the Pareto optimal solutions were finally obtained (Figure 5(a)). A check-in-the-loop of optimal solutions was necessary to evaluate the response surface goodness using CFD (Figure 5(b)): the best-so-far optimum individuals from the response surface were taken and verified using a dedicated CFD simulation, then inserted back in the DOE, which in turn updated the response surface, from which a new Pareto front was obtained. The loop was kept running until a stable and invariant Pareto optimal set was determined. It is worth mentioning that, during the loop iterations, the response surface method allowed for an adaptive refinement in the search regions around maximum C_P and minimum C_D so as to make it possible to have a wider and more uniform Pareto front.

3. Results and discussion

The final Pareto front is depicted in Figure 6, from which a subset of relevant configuration could be extracted: the baseline solution is marked with a black diamond, while optimum for C_D, optimum for C_P and a good compromise between C_D and C_P are marked using a red triangle, a yellow circle and a green square respectively. Performance figure of optimized individuals are given in Figure 6(b). The solution corresponding to minimum C_D (Candidate 1) features a reduction count $\Delta C_D = -0.0254$ (i.e. – 2.54 percentage point reduction), while the one corresponding to maximum C_P (Candidate 3) shows $\Delta C_P = +0.0574$ (i.e. + 5.7 percentage point improvement).

Preprints (www.preprints.org) | NOT PEER-REVIEWED | Posted: 21 August 2020 doi:10.20944/preprints202008.0477.v1

Table 2. Optimization results: Pareto solutions.

	C_d	C_p
Baseline	0.0851	0.9186
Candidate 1	0.0597	0.8974
Candidate 2	0.0634	0.9300
Candidate 3	0.0702	0.9347

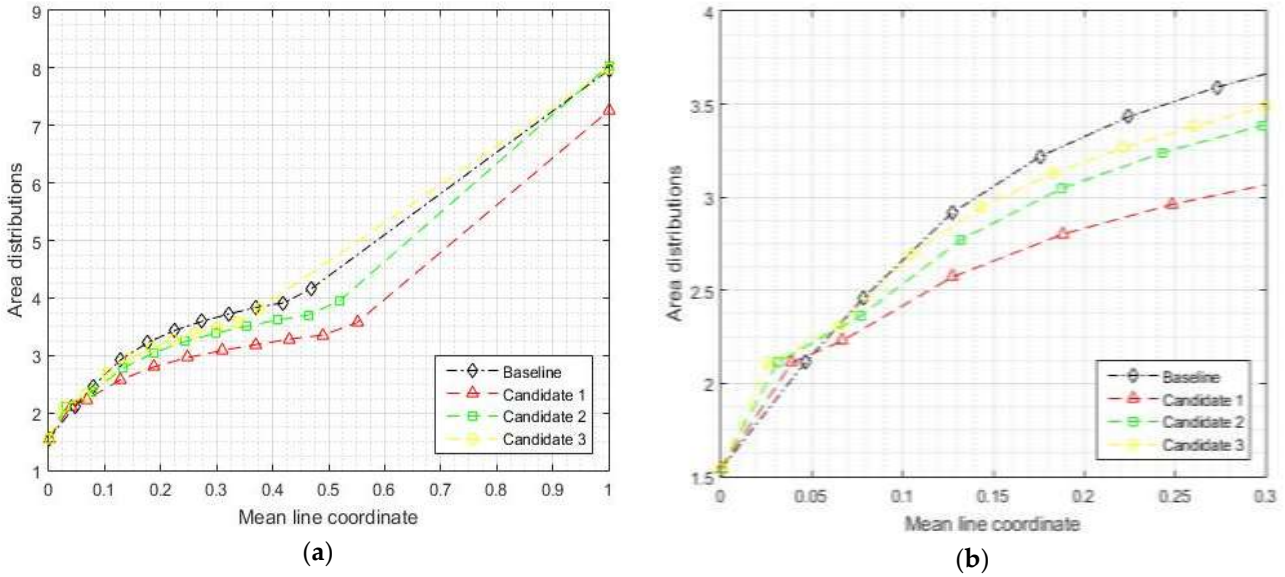

Figure 7. Optimization results: (**a**) Area distribution (**b**) Close up in the range $x \in [0;0.3]$

Figure 8. Comparison among geometries in meridional view: Baseline (grey), Candidate 1 (red), Candidate 2 (green), Candidate 3 (yellow).

3.1. Optimal draft tube configurations

In Figure 7, the area distribution along the meanline coordinate for the Pareto-optimal subset of solutions, compared to the baseline one, is given. It can be seen that optimal solutions exhibit a much lower increase in the area distribution from the beginning of the draft the tube (meanline coordinate > 0.05, see Figure 7(b)): this is beneficial to limit adverse phenomena during flow diffusion in this zone, as confirmed also from the distribution of Cd versus the meanline coordinate (Figure 8(a)), particularly visible in the case of Candidate 1.

In figure 8, a detailed comparison between the performance between optimal solutions and the baseline is presented. It can be seen that for the first draft tube part (until the 20% of the mean line) very similar characteristics can be observed, while the most remarkable differences are visible in the

Preprints (www.preprints.org) | NOT PEER-REVIEWED | Posted: 21 August 2020 doi:10.20944/preprints202008.0477.v1

elbow and in the last part. Candidate 1 has a very similar geometry compared to the baseline, while candidate 2 features an elbow with a much higher radius of curvature. Candidate 3, on the other hand, has much larger dimensions than the baseline and this has a major impact on the excavation costs. As will be seen later, candidate 2 is the best in performance and this is due to the shape of the elbow, a fact that emphasizes the importance of producing a good design in the region where a big part of the diffusion is realized by the draft tube.

3.2. Post-check validation on full machine and result transposition

A number of Pareto optimal draft tubes geometries were obtained from the optimization which were subsequently analyzed *a posteriori*, by connecting them into the CFD model of the entire machine so as to assess their influence on the critical plant characteristics, such as mechanical power and efficiency. In Figure 9, both C_D and C_P of the optimal draft tube geometries are plotted as functions of the mean line coordinate as a result of the calculations using the full CFD model of the turbine.

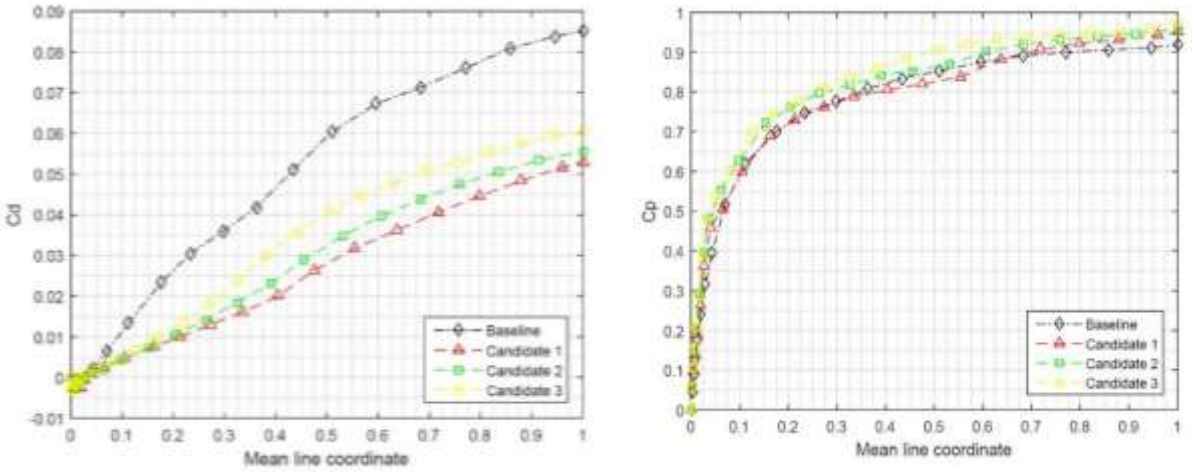

Figure 9. Post check results on draft tube performance using full machine model: (**a**) C_D distribution (**b**) C_P distribution

Table 3. Full machine CFD results (transposed based on baseline CFD results)

CFD	Q'v [m³/s]	H [m]	η/η baseline	η variation [%]	P/P baseline	P variation [%]
Baseline	9.251	5.88	100	/	100	/
Candidate 1	9.286	5.88	100.57	+0.57	100.957	+0.96
Candidate 2	9.323	5.88	101.00	+1.00	101.790	+1.79
Candidate 3	9.281	5.88	100.53	+0.53	100.856	+0.86

The CFD analyses performed on the full machine return different values for the turbine performance figures, especially for the net head and mass flow rate (Table 3). For a better comparison, a results transposition was carried out according to the European IEC EN 60041:1991 standard [16]. In particular, the mass flow rate and the power output data were transposed using the baseline net head. This was acceptable since the condition $0.99 < \sqrt{H}/\sqrt{H'} < 1.01$ on head H' compared to baseline H has been met for each candidate. As can be seen, optimal candidate solutions lead to greater power and efficiency values compared to the baseline. In particular, candidate no. 2 emerges featuring an increment of 1,8% on power produced and 1% on the efficiency ratio.

Preprints (www.preprints.org) | NOT PEER-REVIEWED | Posted: 21 August 2020 doi:10.20944/preprints202008.0477.v1

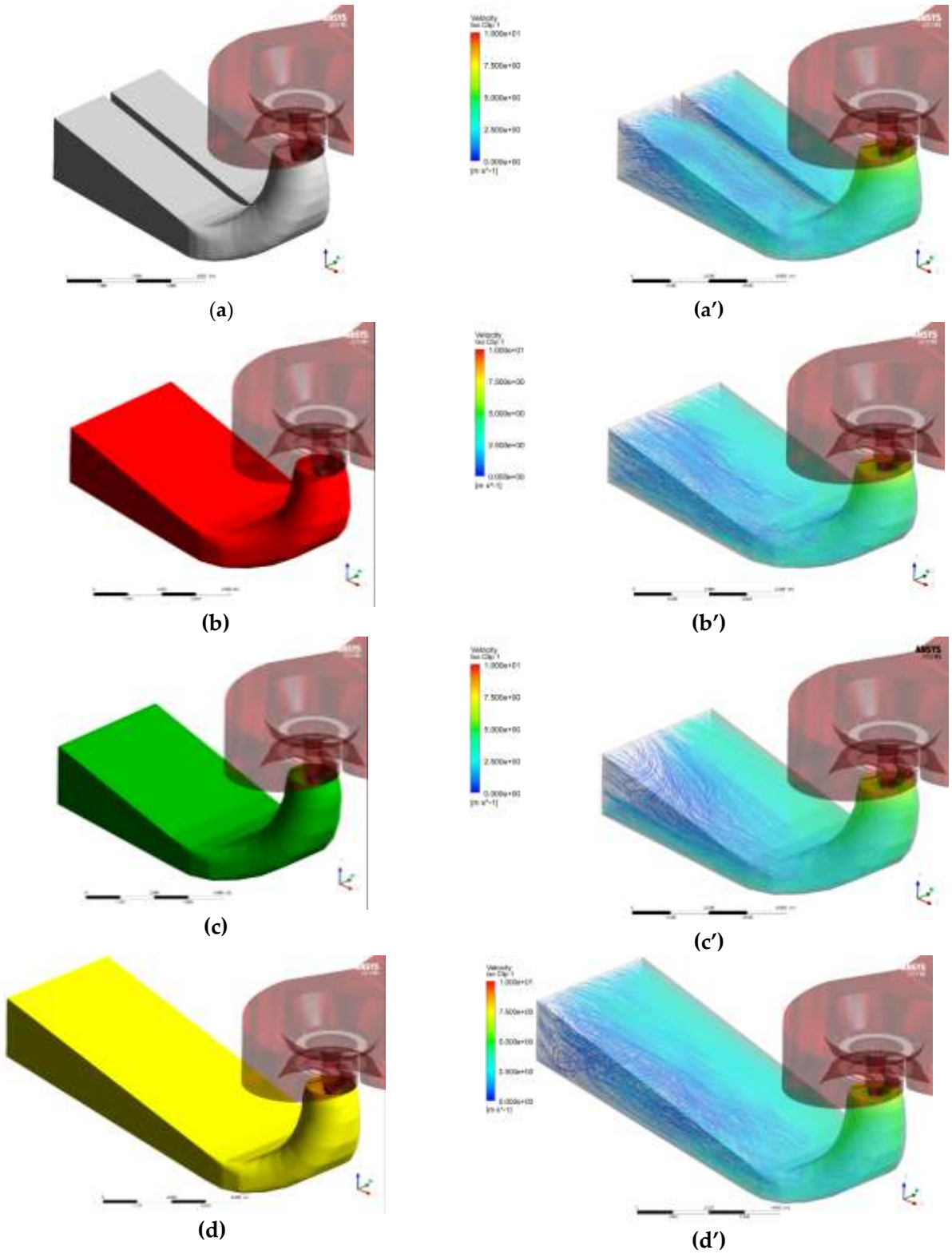

Figure 10. Comparison among geometries (left column), and streamlines colored by velocity (right column): (**a,a′**) Baseline, (**b,b′**) Candidate 1, (**c,c′**) Candidate 2, (**d,d′**) Candidate 3.

Preprints (www.preprints.org) | NOT PEER-REVIEWED | Posted: 21 August 2020 doi:10.20944/preprints202008.0477.v1

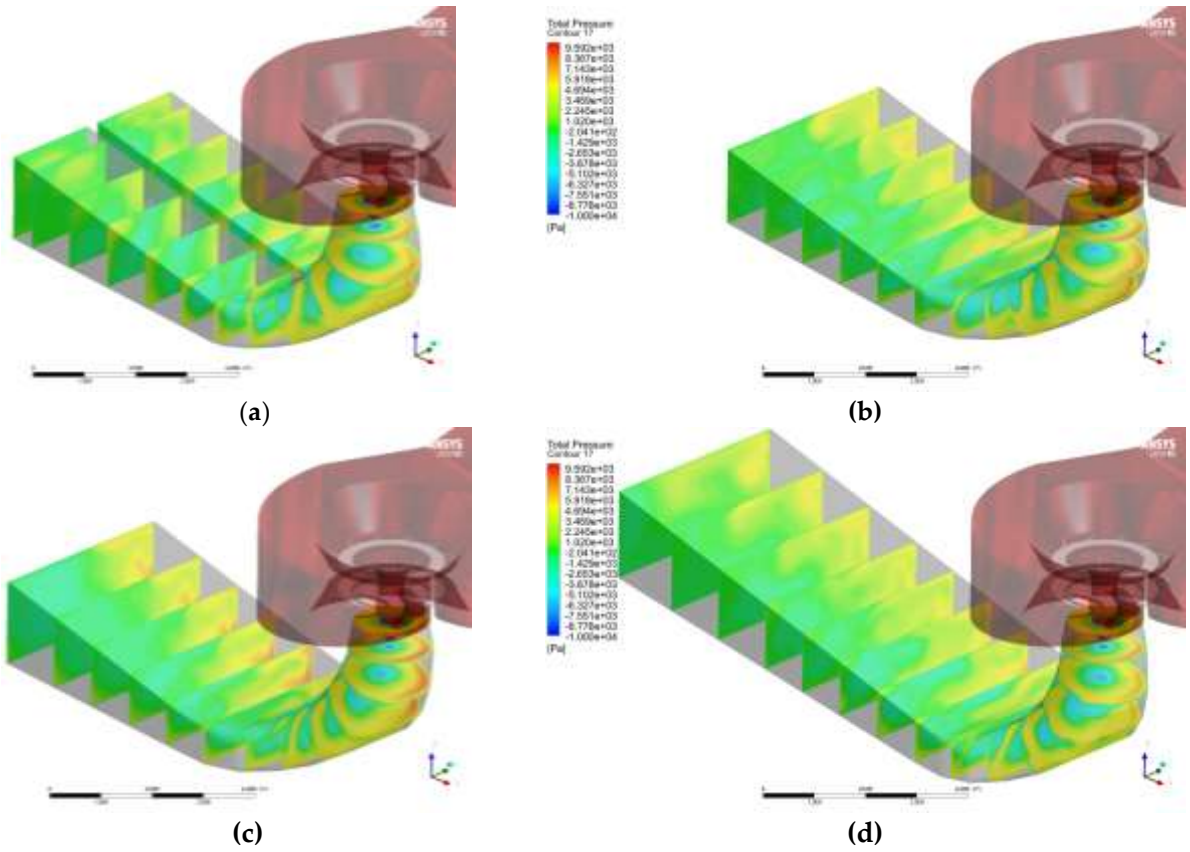

Figure 11. Comparison among relative total pressure distributions: (**a**) Baseline, (**b**) Candidate 1, (**c**) Candidate 2, (**d**) Candidate 3.

From a geometrical point of view (Figure 9), candidates 1 and 2 are not that far from the baseline although they clearly exhibit an elbow shape having a larger radius of curvature, which eventually leads to the exit station of both the elbows and the draft tubes to be placed further downstream with respect to the baseline. Also, candidate number 3 features the same global tendencies, with however a much longer draft tube which eventually would lead to higher installation costs.

From a fluid dynamic standpoint, it is apparent that the largest part of the pressure recovery takes place in the first part of the diffuser (Figure 8), the fact that confirms the importance of having a very accurate design of the region upstream of the elbow. As a matter of fact, approximately 70% of the pressure recovery is realized in the first 20% length of the diffuser. This holds true also for the total pressure losses, which are primarily generated in this region (see Cd behavior in Figure 8, where the largest slope is evidenced in the Cd distribution in the first 20% length of the baseline geometry); localized losses accumulate all along the draft tube meanline, finally leading to overall large Cd value in the baseline. Such an observation has been clearly pointed out also in [5] and [13]: therefore, this study confirms those findings. Furthermore, by looking at total pressure distribution on consecutive station cuts along the draft tube (Figure 11, right column), it is evident that the rotational region at the lowest total pressure in the core of the discharge flow is of a much lower intensity in the optimized solutions compared to the baseline, despite the latter does have a separation wall in the middle of the diffuser. In fact, the analyses carried out have shown that the vortex rope greatly influences the draft tube performance, creating instabilities and turbulent zones in the flow field.

5. Conclusions

A validated CFD model of a draft tube of a Kaplan turbine has been successfully implemented and used for a multi objective optimization based on the construction of a response surface. Two Pareto-optimal designs have been extracted from the final set which overperformed the baseline. Regarding the performance of the draft tube alone, optimum for C_D features a reduction count of –

0.0254 (– 2.54 percentage point reduction), while optimum for C_P shows an incremental count of +0.0574 (i.e. + 5.7 percentage point improvement) with respect to the baseline geometry. A post-check carried out including the optimized draft tubes in the overall turbine confirmed the optimization trends, although the best improvements in terms of delivered hydraulic power – in the case where the overall turbine was considered – have been registered including a third type of diffuser which exhibited an increment of 1,8% in the power produced. Regarding the three best candidate overall, they are slightly deeper than the baseline in terms of excavation dimensions, so a cost/benefit assessment will be needed to determine which is the most appropriate draft tube for a given plant.

Author Contributions: For research articles with several authors, a short paragraph specifying their individual contributions must be provided. The following statements should be used "Conceptualization, E.B. and R.O.; methodology, R.O., E.B.; software, R.O.; validation, R.O., M.M. and R.B.; formal analysis, writing—original draft preparation, R.O.; writing—review and editing, E.B.; supervision, E.B.. All authors have read and agreed to the published version of the manuscript."

Funding: Please add: "This research received no external funding"

Conflicts of Interest: "The authors declare no conflict of interest."

References

1. Kovalev, N.N. *Hydroturbines Design and Construction*, Israel Program for Scientific Translation, Jerusalem 1965.
2. Krivchenko, G. I. *Hydraulic Machines Turbines and Pumps,* CRC-Press, 2nd Ed., 1994.
3. McNabb, J.; Devals, C.; Kyriacou, S. A.; Murry N.; Mullins, B. F. CFD based draft tube hydraulic design optimization. In *Proceedings of the 27th IAHR Symposium on Hydraulic Machinery and Systems*, Editor N. Désy - IOP Publishing, 2014.
4. Marjavaara, B.D. CFD Driven Optimization of Hydraulic Turbine Draft tubes using Surrogate Models. PhD thesis. Lulea University of Technology, Sweden, 2006.
5. Li, Y.; Liu, Q. Analysis of hydraulic performance for Kaplan turbine components based on CFD simulation. In *Proceedings of the IOP Conference Series: Earth and Environmental Science*. Volume 510, Issue 2, 13 July 2020.
6. Brijkishore; Khare, R.; Prasad, V. Performance Evaluation of Kaplan Turbine with Different Runner Solidity Using CFD. In *Advances in Intelligent Systems and Computing*, Book Series, Volume 949, 2020, Pages 757-767.
7. Liu, K.; Yang, F.; Yang, Z.; Zhu, Y.; Cheng, Y. Runner lifting-up during load rejection transients of a Kaplan turbine: Flow mechanism and solution. *Energies* **2019**, 12(24), Article no. 4781.
8. Jošt, D.; Škerlavaj, A.; Lipej, A. Improvement of Efficiency prediction for a Kaplan Turbine with Advanced Turbulence Models. *Strojniski Vestnik J Mech Eng* **2014**, *60(02)*, 124-134.
9. Lyutov, A.E.; Chirkov, D.V.; Skorospelov, V.A.; Turuk, P.A.; Cherny, S.G. Coupled Multipoint Shape Optimization of Runner and Draft Tube of Hydraulic Turbines. *J. Fluids Eng.* **2015**, *137(11)*, 111302 (11 pages).
10. Ciocan, T.; Susan-Resiga, R.; Muntean, S. Improving draft tube hydrodynamics over a wide operating range. *J. Hydraul. Res.* **2016**, *54(1)*, 74-89.
11. Eisinger, R.; Ruprecht, A. Automatic shape optimization of hydro turbine components based on CFD. 2002, Available online at http://kwk.ihs.uni-stuttgart.de/fileadmin/IHS-Startseite/veroeffentlichungen/v2001_05.pdf (accessed on 10 June 2020).
12. Puente, L. R.; Reggio, M.; Guibault, F. Automatic Shape Optimization of a Hydraulic Turbine Draft Tube. In *Proceedings of the IOP Conference Series: Earth and Environmental Science*, 2018, 136, 012019.
13. Sosa, J.B.; Urquiza, G.; Garcìa J.C.; Castro L.L. Computational fluid dynamics simulation and geometric design of hydraulic turbine draft tube. *Adv. Mech. Eng.* **2015**, 7(10), 1–11.
14. Schiffer, J.; Benigni H.; Jaberg, H. An analysis of the impact of draft tube modifications on the performance of a Kaplan turbine by means of computational fluid dynamics. *Proc Inst Mech Eng C J Mech Eng Sci* **2017**, 232(11), 1937-1952.
15. ANSYS CFX -Theory Guide v 19.3 https://ansyshelp.ansys.com/account/secured?returnurl=/Views/Secured/corp/v193/cfx_thry/cfx_thry.html

16. IEC 60041:1991. Field acceptance tests to determine the hydraulic performance of hydraulic turbines, storage pumps and pump-turbines. International Standard. Third edition, 1991-11.
17. Kim, K.-Y.; Samad, A.; Benini, E., *Design optimization of Fluid Machinery*, Wiley, 2019.
18. M. B. Salem, O. Roustant, F. Gamboa, L. Tomaso. Universal Prediction Distribution for Surrogate Models, 2015, Available online at https://arxiv.org/pdf/1512.07560.pdf (accessed on 10 June 2020).